INTRACLUSTER AND INTRAGROUP ENTROPY FROM QUASAR ACTIVITY

A. LAPI AND A. CAVALIERE
Dipartimento di Fisica, Universita "Tor Vergata," Via della Ricerca Scientifica 1, I-00133 Rome, Italy

AND

N. MENCI
INAF–Osservatorio Astronomico di Roma, Sede di Monteporzio Catone, Via di Frascati 33, I-00044 Monteporzio Catone, Italy

ABSTRACT

We investigate how the hierarchical merging of dark matter halos, the radiative cooling of baryons, and the energy feedback from supernovae and active galactic nuclei or quasars combine to govern the amount and the thermal state of the hot plasma pervading groups and clusters of galaxies. We show that, by itself, supernova preheating of the external gas flowing into clusters falls short of explaining the observed X-ray scaling relations of the plasma luminosity L_X or the plasma entropy K versus the X-ray temperature T. To account for the scaling laws from rich to poor clusters takes preheating enhanced by the energy input from active galactic nuclei. In groups, on the other hand, the internal impacts of powerful quasars going off in member galaxies can blow some plasma out of the structure. So they depress L_X and raise K to the observed average levels; meanwhile, the sporadic nature of such impulsive events generates the intrinsic component of the wide scatter apparent in the data. The same quasar feedback gives rise in groups to entropy profiles as steep as observed, a feature hard to explain with simple preheating schemes. Finally, we argue a close connection of the L_X-T or the K-T relation with the $M_\bullet$-σ correlation between the host velocity dispersion and the masses of the black holes, relics of the quasar activity.

Subject headings: galaxies: clusters: general — quasars: general — X-rays: galaxies: clusters

1. INTRODUCTION

The hot medium pervading many single galaxies and most groups and clusters shines in X rays by thermal bremsstrahlung and line emission (see Sarazin 1988). Simple conditions are found to prevail in rich clusters.

These emit huge powers, $L_X \propto n^2 \sqrt{T} R^3 \sim 10^{44}$–$10^{45}$ ergs s^{-1}, in X rays; the temperatures $kT \approx 5$ keV, measured from the continuum and from high excitation lines, are close to the virial values, $kT_v \approx GMm_p/10R$, in the gravitational wells mainly provided by dark matter (DM) masses $M \approx 10^{15}\ M_\odot$ within sizes R of a few Mpc.[1] The inferred gas number densities decline outward from central values $n \approx 10^{-3}$ cm^{-3}; so this medium with low n and high T satisfying $kT/e^2 n^{1/3} \sim 10^{12}$ constitutes the best ion-electron plasma in the universe ever, the intracluster *plasma* (ICP).

Such a medium is apparently *simple* on the following accounts. Microscopically, it is constituted by pointlike particles in thermal equilibrium. At the macroscopic end, the overall baryonic fractions resulting from the ICP densities and radial distributions inventoried in many clusters (White et al. 1993; Allen & Fabian 1994) come to values $m/M \approx 0.16$; this is close to the cosmic ratio Ω_b/Ω_M of baryons to DM obtained in the current concordance cosmology from the parameters $\Omega_b \approx 0.044$ and $\Omega_M \approx 0.23$ (see Bennett et al. 2003).[2] In addition, the chemical composition is reasonably constant from cluster to cluster, and close to one-third of the solar value (see Matteucci 2003).

However, surprises arise in moving from rich clusters toward poor groups. In fact, similarly simple conditions holding in the intragroup plasma (IGP) would imply that the luminosities retain the gravitational scaling $L_X \propto T^2$ (Kaiser 1986). This would apply if the IGP passively followed the DM evolution and retained the key cluster behaviors: $m/M \approx$ const, i.e., densities n proportional to the DM mass density ρ, and temperatures T close to the virial value $T_v \propto M/R \propto M^{2/3}\rho^{1/3}$.

Instead, the luminosities recently detected or revised (Horner 2001; O'Sullivan et al. 2003; Osmond & Ponman 2004) are lower by factors of 10^{-1} to 10^{-2}; see Figure 1. The figure also shows how the emissions from poor groups and large galaxies scatter widely and often downward, a feature of a largely intrinsic nature (Mushotzky 2004).

So in such smaller structures the plasma is surprisingly underluminous and hence *underdense*. This is an even more surprising result, considering that in the standard hierarchical cosmogony (see Peebles 1993) such earlier condensations ought to be denser, if anything. Moreover, for $kT < 2$ keV the pinch of highly excited metals contributes important line emissions that imply a flatter $L_X \propto T$, if anything. How the observed steep decrease may come about constitutes a widely debated issue.

Our proposal centers on the energy gained or lost by the baryons through several processes: the gravitational heating driven by the merging events that punctuate the hierarchical growth of DM condensations ("halos"; see Peebles 1993); the radiative cooling of the baryons; and the energy fed back to baryons when they partly condense within galaxies into massive stars then exploding as Type II supernovae (SNe), or accrete onto a central supermassive black hole (BH) energizing an active galactic nucleus (AGN) or a quasar.

This paper is organized as follows. In § 2 we use a telling quantity, the plasma entropy, to show that energy feedback from astrophysical sources is needed to explain its high levels in poor clusters and groups. In § 3 we show that preheating by SNe alone is not enough. In § 4 we consider preheating

---

[1] Throughout the paper k is the Boltzmann constant, G is the gravitational constant, m_p is the proton mass, and e is the electron charge.

[2] This will be used throughout the paper, with its additional parameters $\Omega_\Lambda \approx 0.73$ for the dark energy density and $H_0 \approx 70\ h_{70}$ km s^{-1} Mpc^{-1} for the Hubble constant.
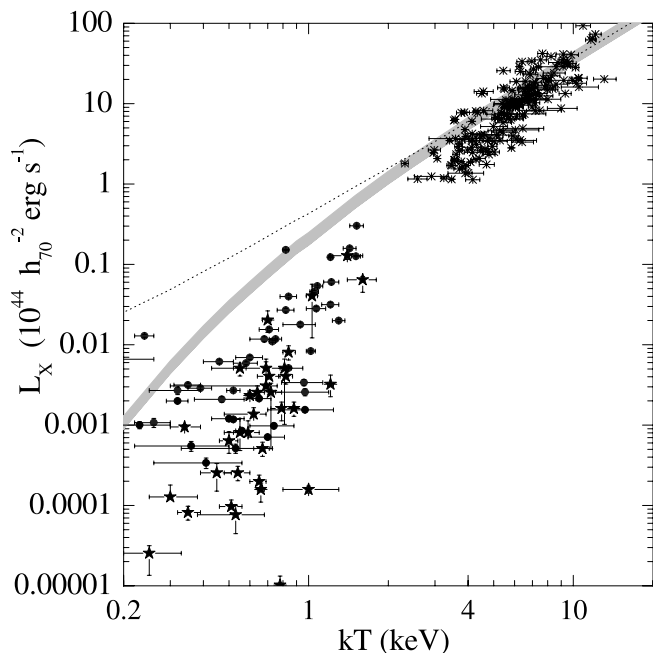
FIG. 1.—Integrated X-ray luminosity L_X vs. X-ray temperature T. Data for clusters (*crosses*) are from Horner (2001), for groups (*circles*) from Osmond & Ponman (2004), and for early-type galaxies (*stars*) from O'Sullivan et al. (2003). The dotted line represents the gravitational scaling, with line emission included. The strip (with 2 σ width provided by the merging histories) illustrates our results for SN preheating with $k\Delta T = \frac{1}{4}$ keV per particle, as discussed in § 3.
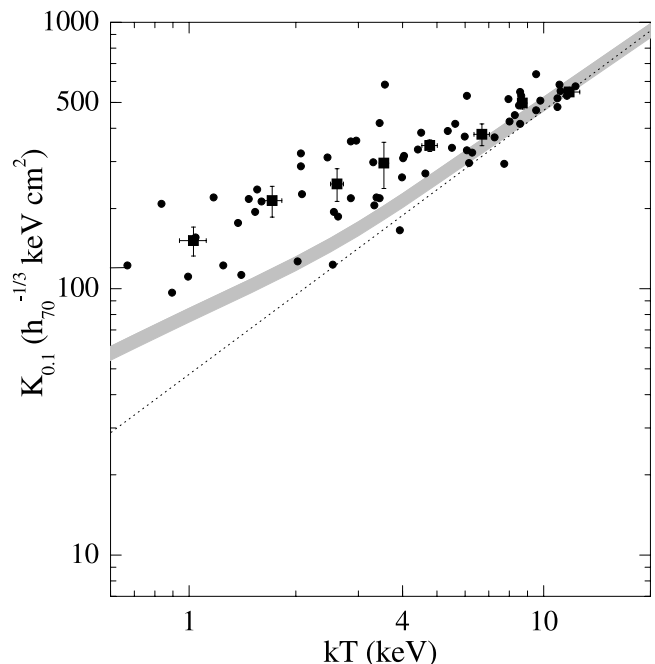

FIG. 2.—Central entropy $K_{0.1}$ (at $r \approx 0.1R$) vs. X-ray temperature T. Data for clusters and groups are from Ponman et al. (2003): Circles mark individual systems, and squares refer to binned data. The dotted line represents pure gravitational heating. The strip (with 2 σ width provided by the merging histories) illustrates our results for SN preheating with $k\Delta T = \frac{1}{4}$ keV per particle, as discussed in § 3.

enhanced by AGNs, compute the resulting X-ray scaling relations, and critically discuss the outcomes of this approach. In § 5 we also consider the internal impacts from quasars; we compute their effect on the X-ray scaling relations and on the entropy profiles in groups and show how these solve the shortcomings of all external preheating scenarios. In § 6 we highlight and discuss the main features of our comprehensive approach.

Auxiliary computations and derivations are given in the Appendices. In Appendix A we derive equation (2) of the main text from the hydrostatic equilibrium and give handy approximations. In Appendix B we reformulate the classic Rankine-Hugoniot jump conditions in a general form that is also valid for accretion shocks/layers and derive equations (5) and (6) of the main text. In Appendix C we develop a new family of self-similar hydrodynamic solutions describing the blast waves driven by the internal impacts of quasars and extensively used in § 5.

2. X-RAY LUMINOSITY AND ENTROPY

This paper deals with the energy budget of the baryons. The latter experience *gravitational* heating to $T \approx T_v$ (discussed in detail in § 4) as they fall into the hierarchically growing DM structures. *Nongravitational* energy losses or inputs deplete the baryon density; this is because losses trigger baryon condensation to stars, while inputs cause outflow from and hinder inflow into newly forming structures.

All such processes are probed with the adiabat $K \equiv kTn^{-2/3} \propto e^{2s/3k}$, a direct measure of the specific entropy s (see Bower 1997; Balogh et al. 1999). The levels of the adiabat K are linked to L_X by the inverse relation

$$K \propto L_X^{-1/3} T^{5/3}, \qquad (1)$$

which obtains at $z \approx 0$ on eliminating n between their respective expressions; note that $T^{5/3}$ goes over to $T^{4/3}$ for important line emission, and that we are neglecting the weakly T-dependent shape factors for K and $L_X^{1/3}$.

Clearly, K stays constant under adiabatic transformations of the plasma. Gravitational heating would set the scaling $K \propto T$ (corresponding to $L_X \propto T^2$ after eq. [1]), but Figure 2 shows the data for decreasing T to deviate substantially upward; this indicates that additional nongravitational processes occurred during a structure's merging history. The present paper investigates how these processes affect the adiabat $K = K_2\kappa(r)$, namely, the level K_2 at the virial radius $r = R$ and the inner profile $\kappa(r)$.

The relation of these quantities to the density run $n(r)$ of the plasma in hydrostatic equilibrium is derived in Appendix A and reads

$$\frac{n(r)}{n_2} = \kappa^{-3/5}(r)\left[1 + \frac{2}{5}\beta \int_r^R dr' \frac{d\phi}{dr'} \kappa^{-3/5}(r')\right]^{3/2}; \quad (2)$$

the boundary condition at $r = R$ is given by $n_2 = (kT_2/K_2)^{3/2}$, but K_2 will be related to T_2 in § 4. The parameter $\beta = T_v/T_2$ is the ratio of the DM to the thermal plasma scale height in the gravitational potential $\phi(r)$; the latter is normalized to the one-dimensional dispersion $\sigma^2 \equiv kT_v/\mu m_p$, with $\mu \approx 0.6$ for the nearly cosmic composition of the plasma (Cavaliere & Fusco-Femiano 1976). For a polytropic entropy distribution $\kappa(r) \propto n(r)^{\Gamma-5/3}$ with uniform index $\Gamma \equiv 5/3 + d \ln \kappa/d \ln n$, equation (2) yields the familiar form $n = n_2[1 + (\Gamma - 1)\beta\Delta\phi/\Gamma]^{1/(\Gamma-1)}$ in terms of the potential drop $\Delta\phi$ inward of R; the isothermal limit $n = n_2 e^{\beta\Delta\phi}$ for $\Gamma = 1$ provides the standard model to fit the X-ray surface brightness profiles, which yields values $\beta \approx 0.7$ in rich clusters. In particular, we use equation (2) to compute integrated

luminosities $L_X \propto \int dr \, r^2 n^2(r) T^{1/2}(r)$ and central entropies $K_{0.1}$ at $r = 0.1R$, which we compare with the data.

Throughout the paper we will make use of "semianalytic" techniques. This is because the nongravitational processes affecting K include energy inputs and radiative losses, which interplay in complex patterns with gravitational heating; so even numerical simulations based on advanced N-body and hydrocodes are driven to, or beyond, their present limits and have to borrow from semianalytic models much subgrid physics (see discussion by Borgani et al. 2002).

Concerning radiative losses, they do operate within galaxies to remove low-entropy gas by condensing it into stars, a process that we include in our semianalytic modeling. But extensive cooling as needed to substantially raise the residual ICP/IGP entropy or depress L_X would produce too many unseen stars (see Voit & Bryan 2001; Sanderson & Ponman 2003). On the other hand, cooling triggers catastrophic instabilities unless closely restrained by other processes feeding energy back to baryons (see Blanchard et al. 1992); so energy *additions* $\Delta E > 0$ are mandatory anyway and will constitute our focus next.

3. THE NEED FOR AGN FEEDBACK

Obvious energy sources are provided by Type II SN explosions; do they contribute enough energy feedback? SNe provide energies $E_{SN} \approx 10^{51}$ ergs with an occurrence $\eta_{SN} \lesssim 5 \times 10^{-3}$ per solar mass condensed into stars, the latter value being calibrated so as to include the yield of strong winds from young hot stars (Bressan et al. 1994).

Such outputs may be coupled to the surrounding gas at levels $f_{SN} \lesssim \frac{1}{2}$ when cooperative SN remnant propagation takes place, as in the case of starbursts, to drive subsonic galactic winds (see Matteucci 2003). Then the integrated thermal input attains the maximal level (Cavaliere et al. 2002),

$$k\Delta T = \frac{2}{3} \frac{\mu m_p}{} f_{SN} E_{SN} \eta_{SN} \frac{m_*}{m} \lesssim \frac{1}{4} \text{ keV particle}^{-1}, \quad (3)$$

in groups with stellar to gas mass ratios up to $m_*/m \approx \frac{1}{2}$ (see David 1997); somewhat smaller values obtain in clusters (e.g., Lin et al. 2003).

The SN feedback and the originating star formation are described by semianalytic models, in particular that of Menci & Cavaliere (2000). They base their model on the DM merging histories, i.e., the hierarchical buildup of a galaxy or a group with their baryonic contents through merging events with comparable or smaller partners, down to nearly smooth inflow (Lacey & Cole 1993). The model, in addition, specifies how the baryons are cycled between the cool, stellar, and hot phases; the latter contributes to the ICP/IGP, while the former two phases yield the stellar observables .

It is found that most of a structure's DM mass M (and of the IGP mass likewise) is contributed to its main progenitor by merging partners with masses $M' \lesssim M/3$ and related virial temperatures $T'_v \lesssim 0.6 T_v$ (Cavaliere et al. 1999). The smaller lumps have shallower gravitational wells and produce more star-related energy on scales closer to their dynamical times; so they are more effective in heating up their gas share to temperatures $T'_v + \Delta T$. During each subsequent step of the hierarchy forming larger groups or clusters, the *externally* preheated gas (see Muanwong et al. 2002) will be hindered from flowing in and contributing to the IGP or ICP. So under any model depleted densities will be propagated some steps *up* the hierarchy.

In sum, SNe make optimal use of their energy in *preheating* the IGP. However, their input $k\Delta T \approx \frac{1}{4}$ keV per particle turns out to cause only limited luminosity depressions or entropy enhancements, as shown by the light strips in Figures 1 and 2. The result may be understood by referring to the simple isothermal case where $L_X \propto n_2^2 \int dr \, r^2 e^{2\beta\Delta\phi}$ applies; in moving from rich to poor clusters n decreases, governed mainly by the decreasing exponential $e^{2\beta\Delta\phi}$ (as visualized by Fig. 5 of Cavaliere & Lapi 2005). But the normalized DM potential $\Delta\phi$ deepens because of the increased concentration (an intrinsic feature discussed in Appendix A). To offset this trend and to provide constant or decreasing density, it is clearly required that $\beta \approx T_v/(T_v + \Delta T)$ be lowered from the cluster value by a sufficiently strong preheating ΔT; in particular, the approximation $\beta \approx 0.7 - \Delta T/T$ holds; see Appendix B and specifically equation (B9) with $\theta = T/\Delta T$. Numerically, the requirement comes to $k\Delta T > 0.5$ keV per particle for any significant luminosity depression in a poor cluster; yet more preheating is required with polytropic plasma distributions. On the other hand, including Type Ia SNe still does not meet the above requirement (see Pipino et al. 2002).

In view of these SN limitations, in the rest of the paper we concentrate on the stronger feedback provided by quasars and AGNs (see Valageas & Silk 1999; Wu et al. 2000; Yamada & Fujita 2001; Nath & Roychowdhury 2002). These sources are kindled when sizeable amounts of galactic gas, triggered by mergers or interactions of the host with companion galaxies, are funneled downward from kiloparsec scales; they not only form circumnuclear starbursts but eventually trickle farther down to the very nucleus (see Menci et al. 2004) and accrete onto a central supermassive BH.

4. EXTERNAL PREHEATING FROM AGNs

On accreting the BH mass $M_\bullet$, the integrated energy input to the surrounding plasma comes to values of

$$k\Delta T = \frac{2\mu m_p}{3} f \eta c^2 \frac{M_\bullet}{4M_b} \frac{m_*}{m} \approx \frac{1}{2} \text{ keV particle}^{-1}, \quad (4)$$

easily larger than for SNe. We have used the standard mass-energy conversion efficiency $\eta \approx 10^{-1}$ and the locally observed ratio $M_\bullet/M_b \approx 2\times10^{-3}$ of BH to galactic bulge masses (Merritt & Ferrarese 2001); the factor $\frac{1}{4}$ accounts for the bulge mass observed in blue light compared to that integrated over the star formation history (Fabian 2004a). Finally, we will adopt values $f \approx 5\times10^{-2}$ for the fractional AGN output actually coupled to the surrounding gas, on the grounds discussed next.

The 10% radio-loud AGNs directly produce considerable kinetic or thermal energies in the form of bubbles and jets (see Forman et al. 2004), but statistics and nonspherical geometry reduce their average contribution to f. On the other hand, in the 90% radio-quiet AGNs a small coupling is expected for the radiative output because of the flat spectrum and low photon momenta; the observations of wind speeds up to $v_w \approx 0.4c$ suggest values around $v_w/2c \approx 10^{-1}$ associated with covering factors of order 10^{-1} (see Chartas et al. 2003; Pounds et al. 2003). We see that average values around $f \approx 5\times10^{-2}$ are consistent not only with the X-ray observations of the IGP, but also with the mainly optical observations of the relic BHs in galaxies.

Considering that the AGN activity closely parallels the star formation in spheroids (Franceschini et al. 1999; Granato et al. 2004; Umemura 2004), we add the AGN energy injections to
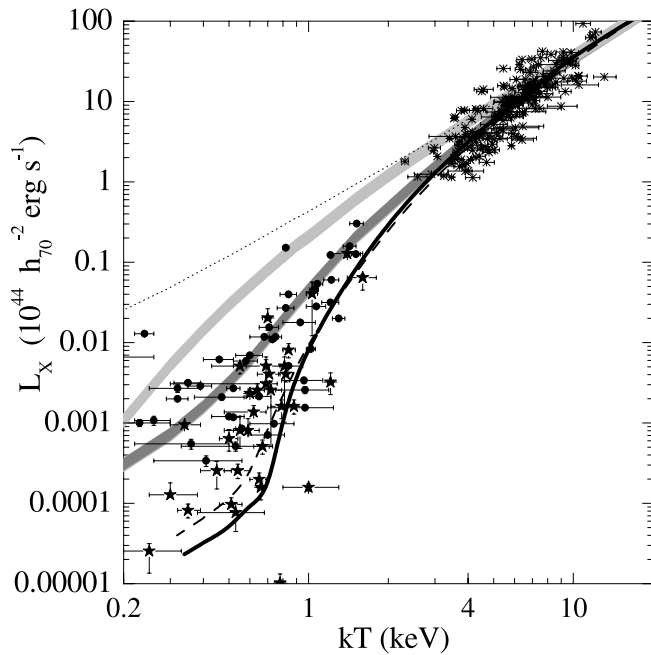
FIG. 3.—Integrated X-ray luminosity L_X vs. X-ray temperature T. Data: Dotted line and light shaded strip are the same as in Fig. 1. The heavy shaded strip (with 2 σ width provided by the merging histories) illustrates our results for external preheating when including the AGN contribution to a total $k\Delta T = \frac{3}{4}$ keV per particle, as discussed in § 4. Our results for the internal impacts from quasars are illustrated by the solid (ejection model) and dashed (outflow model) lines; see § 5 for details. The coupling level of the quasar output to the ambient medium is $f = 5 \times 10^{-2}$.

FIG. 4.—Central entropy $K_{0.1}$ vs. X-ray temperature T. Data: Dotted line and light shaded strip are the same as in Fig. 2. The heavy shaded strip (with 2 σ width provided by the merging histories) illustrates our results for external preheating when including the AGN contribution to a total $k\Delta T = \frac{3}{4}$ keV per particle, as discussed in § 4. Our results for the internal impacts from quasars are illustrated by the solid (ejection model) and dashed (outflow model) lines; see § 5 for details. As before, the coupling level is $f = 5 \times 10^{-2}$.

SNe to obtain preheating energies up to $k\Delta T \approx \frac{3}{4}$ keV per particle. Such a combined value produces a sizeable step toward the locus of the data, as shown in Figures 3 and 4 by the heavy strips. How we obtain these is explained next.

Toward this purpose it is convenient to discuss further the *modus operandi* of the external preheating. During the formation of a DM structure, outer lumps and the associated gas flow in together; but just inside R the smaller and/or less bound gas bunches are promptly stripped away from their DM hosts, while gaining entropy (Tormen et al. 2004; see their Fig. 8). The outcome constitutes a complex patchwork of shocks of all sizes, comprised within an outer *layer* with thickness $\delta \lesssim 10^{-1}R$ wherein most of the entropy rise takes place.

The net result is close to that computed from considering a coherent accretion shock, roughly spherical and located at $r \approx R$ as considered by Cavaliere et al. (1999), Dos Santos & Doré (2002), and Voit et al. (2003). In fact, across the layer we may retrace the classic Rankine-Hugoniot derivation based on the conservation of mass, momentum, and energy for plasma particles with 3 degrees of freedom; for a reasonably thin layer we recover the standard entropy jump across a shock,

$$K_2 = K_1 \theta^{5/3} \left[2(\theta - 1) + \sqrt{4(\theta-1)^2 + \theta} \right]^{-2/3}, \quad (5)$$

to within $O(\delta/R)$ accuracy, *independently* of geometric details (as discussed in Appendix B). To within the same accuracy, the strength parameter $\theta \equiv T_2/T_1$, i.e., the ratio of the down- to the upstream temperature, is linked by

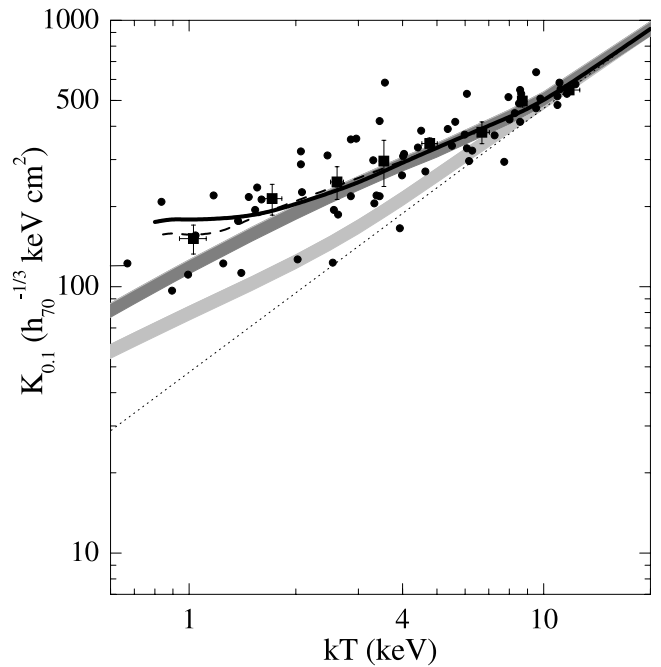$$\theta = \frac{5\mathcal{M}^2}{16} + \frac{7}{8} - \frac{3}{16\mathcal{M}^2} \quad (6)$$

to the Mach number $\mathcal{M} = (3\mu m_p \tilde{v}_1^2 / 5kT_1)^{1/2}$ of the flow velocity $\tilde{v}_1$ relative to the shock/layer. Henceforth we refer to "shocks," but we also include thin layers.

We now consider in closer detail the *combined* preheating by SNe and AGNs; this comes into play through $T_1 = T'_v + \Delta T$ that enters K_1 and θ in equations (5) and (6). We average K_2 over the full structure's merging history that includes the distributions of progenitor masses M' or related T'_v; to this purpose we implement, as in Cavaliere et al. (1999), the conditional probabilities and the merging rates from the standard cold DM cosmogony as given by Lacey & Cole (1993). This straightforward if laborious procedure (which is dominated by the smaller partners and so further validates eqs. [5] and [6], as discussed in Appendix B) is made semianalytically and yields the heavy strips in Figures 3 and 4. Their width illustrates the variance (at 95% probability level) around the mean value, induced mainly by the merging stochasticity; the smooth, low-power AGN activity considered here does not contribute much additional scatter.

Next we discuss why the results fit clusters better than groups. In very *rich* clusters the infall velocities $v_1 \approx 2.1(kT_v/\mu m_p)^{1/2}$ are large, and $\tilde{v}_1 \simeq 4v_1/3$ is larger yet (see Appendix B). These velocities are dominantly supersonic, except for the few major lumps that carry warm gas deep into the structure (as observed by Mazzotta et al. 2002) and contribute little to prompt entropy gains. So the effective shocks are uniformly *strong* with $\theta \simeq \mu m_p v_1^2 / 3kT_1 \gg 1$; see equation (B7). Such conditions in equation (5) yield $K_2/K_1 \simeq \theta/4^{2/3}$, corresponding to nearly constant $n_2/n_1 \approx 4$ (eq. [B7]); they also yield a nearly constant value of $\beta = T_v/\theta T_1 \simeq 3kT_v/\mu m_p v_1^2 \approx \frac{2}{3}$. In other words, here we find pure gravitational heating at work to enforce $K \propto T$ or $L_X \propto T^2$.

The related, raising entropy profiles reflect the history of progressive depositions of shells undergoing stronger and

stronger shocks during the hierarchical growth to a rich cluster; in fact, in the outer regions we find $\kappa \propto r^{1.1}$ and $\Gamma \approx 1.1$. We derive these values by reducing to bare bones the model of Tozzi & Norman (2001). We adopt in full the concordance cosmology and nearly self-similar hierarchical collapse with a constant perturbation power index around -1.2 appropriate for rich clusters (see Padmanabhan 2003); these conditions imply the last accreted shell to add a mass $\Delta M \propto M$ on top of the mass $M \propto (1+z)^{-3.2}$ virialized at $z \gtrsim \frac{1}{2}$ (see also Lapi 2004). In the process, the entropy $K \propto T/n^{2/3}$ grows because the strong shocks prevailing in rich clusters yield not only $T \approx T_v$ and $n_2 \simeq 4n_1$ as above, but also $n_1 \propto \rho \propto (1+z)^{2.9}$ considering the appropriate collapse threshold; in terms of $m \propto M$ this translates into $\kappa \propto m^{2/3}(1+z)^{-1} \propto m$.

For the ICP in equilibrium, the radial entropy profile $\kappa(r)$ corresponding to this distribution $\kappa(m)$ is found as follows. In the outskirts we approximate the entropy profile as $\kappa(r) \propto r^{\alpha}$, with α to be determined; then equation (A3) implies $n(r) \propto r^{-3(\alpha+2)/5}$, and we obtain $\kappa(r) \propto m(<r)^{5\alpha/3(3-\alpha)}$ on considering that $m(<r) = 4\pi m_p \int^r dx\, x^2 n(x)$ holds. Requiring consistency with the entropy distribution $\kappa \propto m$ derived above, we obtain $\alpha \approx 1.1$. So our final results read $\kappa(r) \propto r^{1.1}$ and $n(r) \propto r^{-1.9}$, which accord with the data by Ponman et al. (2003) and with the simulations by Tornatore et al. (2003); the related value $\Gamma \approx 1.1$ agrees with that observed by Ettori & Fabian (1999) and De Grandi & Molendi (2002).

In *poor* clusters, on the other hand, the infall is slower, with $\tilde{v}_1 \simeq 4v_1/3 + 5kT_1/4\mu m_p v_1$; see Appendix B. Now the inflow is *less* supersonic, and the accretion shocks are easily modulated by the preheating temperature to a strength $\theta \simeq \mu m_p v_1^2/3kT_1 + 3/2$; see equation (B8). Less entropy is produced by these intermediate shocks, while an additional contribution is just carried in with the warm inflowing gas, to yield $K_2/K_1 \simeq (\theta + 5/8)/4^{2/3}$; correspondingly, the boundary densities are lowered to $n_2/n_1 \simeq 4-15/4\theta$ (eq. [B8]). In addition, the density profiles are now just flatter than in rich clusters, since $n(r)/n_2$ is appreciably decreased with preheating levels $k\Delta T \approx \frac{3}{4}$ keV per particle that satisfy the condition derived at the end of § 3; these are effective in lowering all densities and hence in depressing L_X and enhancing K.

In *groups* and galaxies these preheating levels are enough to cause smoother, transonic inflows and *weak* shocks with $\theta \simeq 1$, yielding small jumps $K_2/K_1 \simeq 1 + 5(\theta - 1)^3/6$ and $n_2/n_1 \simeq 1$; see equation (B10). The X-ray scaling relations produced by the combined external preheating of SNe and AGNs (Figs. 3 and 4, *heavy strips*) are in marginal agreement with the trends in the data, while the wide scatter is still unaccounted for. Moreover, the weak shocks so produced would imply nearly flat profiles $\kappa(r)$, which often are not observed (Pratt & Arnaud 2003; Rasmussen & Ponman 2004).

The problem with such isentropic profiles would be aggravated and propagated to poor clusters, while the entropy would be raised too much, if one tuned high the AGN preheating, much above the level $\frac{1}{2}$ keV per particle given by equation (4). From the previous relations the problem is easily seen to develop even before solving the luminosity issue in groups.

5. INTERNAL IMPACTS OF QUASARS

But right in groups and galaxies the impulsive inputs by powerful quasars take over, providing from the *inside* an additional impact on the IGP that can cause outflow or ejection. For this to occur, two energies compete: the overall input $\Delta E \approx 2 \times 10^{62} f(M_\bullet/10^9\, M_\odot)(1+z)^{-3/2}$ ergs provided by a quasar on accreting the mass $M_\bullet$ within the host dynamical time
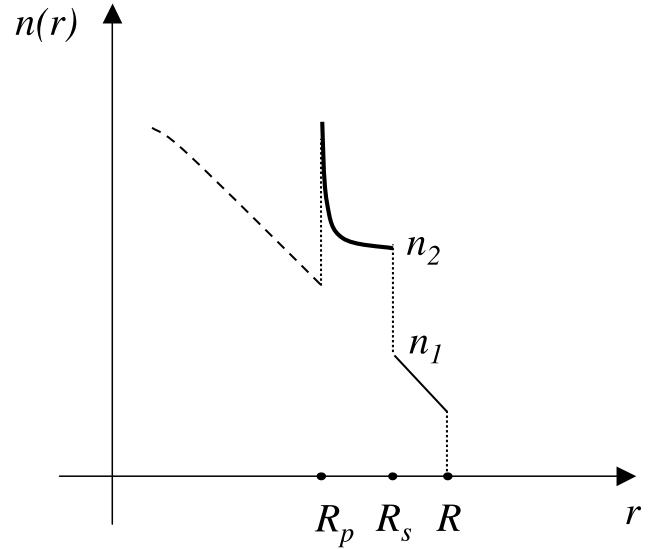

Fig. 5.—Outline of the density distribution during the propagation of a quasar-driven blast throughout the equilibrium plasma. *Dashed line*: Initial density run $n \propto r^{-2}$ in the volume already evacuated by the blast. *Thick solid line*: Perturbed density in the blast (specified in Fig. 6). *Thin solid line*: Still unperturbed density. The perturbed flow is confined between the trailing piston at R_p and the leading shock at R_s; in our illustration, this is still far from the virial radius R.

$t_d \approx 10^8$ yr set by mergers or interactions, and the (absolute) total energy $E \approx 2 \times 10^{61} (kT/\text{keV})^{5/2}(1+z)^{-3/2}$ ergs residing in the equilibrium IGP (Lapi et al. 2003).

The relevant ratio,

$$\frac{\Delta E}{E} \approx 0.5 \frac{f}{5 \times 10^{-2}} \frac{M_\bullet}{10^9\, M_\odot} \left(\frac{kT}{\text{keV}}\right)^{-5/2}, \tag{7}$$

is small in clusters but increases toward groups and approaches unity in poor groups with $kT \approx 1$ keV to attain a few in large galaxies with $kT \approx \frac{1}{2}$ keV. Within the central kiloparsec of such structures the quasar launches a piston (see King 2003; Granato et al. 2004) that drives through the surrounding plasma a blast wave bounded by a leading shock at $r = R_s$ (see Fig. 5). These blasts constitute effective, quasi-isotropic means to propagate energy far away from the central source.

While the latter shines, the blast affects the plasma out to the distance R_s where the initial energy $E(<R_s)$ is comparable to the cumulative input $\Delta E(t)$. In fact, the condition $\Delta E(t)/E(<R_s) = $ const defines the self-similar propagation of the blast and the motion $R_s(t)$ of the leading shock; as shown in Appendix C, the result is $R_s(t) \propto t^{2/\omega}$ in an initial distribution $n(r) \propto r^{-\omega}$ ($2 \leq \omega < 2.5$) for the plasma density under the energy input $\Delta E(t) \propto t^{2(5-2\omega)/\omega}$. The simplest flow obtains with $\omega = 2$ (the standard isothermal sphere), implying a source power $L(t) \equiv d\Delta E/dt = $ const; when $\omega > 2$ applies the power $L(t) \propto t^{5(2-\omega)/\omega}$ declines, a useful means to describe the quasar fading because of its own feedback on the accreting gas.

This new family of hydrodynamic solutions, proposed by Cavaliere et al. (2002), is described in detail in Appendix C; it is used below to evaluate mass loss from, and entropy distribution into, the structures. The solutions include the restraints set to gasdynamics by a nonzero initial pressure $p(r) \propto r^{2(1-\omega)}$ and by the DM gravity; so not only do they imply a well-defined $E(<R_s)$, but they also cover the full range of blast

TABLE 1
RELEVANT BLAST WAVE QUANTITIES ($\omega = 2$)

$\Delta E/E$	$\mathcal{M}$	$\langle p \rangle / p_1$	$1 - \Delta m/m$	β'/β
0.3............................	1.2	3.6	0.92	0.94
1................................	1.5	4.6	0.58	0.86
3................................	1.9	6.3	~ 0	...

strengths from weak in clusters to strong in galaxies, depending on the magnitude of the key parameter $\Delta E/E$.

As $\Delta E/E$ increases, so does the Mach number $\mathcal{M}$ of the leading shock; their relation is shown in Figure 7 and is approximated by $\mathcal{M}^2 \simeq 1 + (\Delta E/E)$ for $\Delta E/E \lesssim 2$ in the simple $\omega = 2$ model. Meanwhile, the ratio of the kinetic to the thermal energy ranges up to 2; see equation (C17). Correspondingly, within the time t_d increasing plasma amounts are driven beyond the virial radius R of a large galaxy or a poor group; in the simple $\omega = 2$ model the fractional mass ejected or flowed out is well approximated by $\Delta m/m \simeq \Delta E/2E$; see also Table 1.

These results turn out to be nearly independent of the specific mode for mass loss; in particular, we compare two extreme cases. In the first one ("ejection"), we take Δm to be the mass in the blast driven outside of the virial radius R at $t = t_d$ by the blast kinetic energy. In the second case ("outflow"), we adopt constant pressure as boundary condition at $r = R$ to obtain new densities $n' \propto (T + \Delta T)^{-1}$; now Δm is the mass flowed out of the structure due to the extrathermal energy ΔT deposited by the blast. Beyond model details, we find that the mass loss closely obeys $\Delta m/m \simeq \Delta E/2E$.

In both cases, after the passage of the blast the IGP will recover hydrostatic equilibrium, described by equation (2). But all new densities n' will be *depleted* by the factor $1 - \Delta m/m$ below the initial value already affected by the preheating from SNe and AGNs. In addition, in both cases the extrathermal energy deposited by the blast lowers the values of β'; this is given in Table 1 and may be understood in terms of $\beta'/\beta \approx T/(T + \Delta T)$. The resulting $L_X \propto (1 - \Delta m/m)^2$, including the appropriate T-dependent shape factor, is shown by the solid and the dashed lines in Figure 3 for both models, ejection and outflow, discussed above.

The IGP entropy is increased by quasar-driven blasts. While these sweep through the plasma, a moderate production takes place across the leading shock and leads to a jump K_2/K_1 given again by the general equations (5) and (6). In the equilibrium recovered after the plasma mass loss $\Delta m/m$ caused by ejection or outflow, the entropy is further enhanced to read

$$K_2'/K_2 = (1 - \Delta m/m)^{-2/3}. \qquad (8)$$

For example, in a group with $kT = \frac{3}{4}$ keV the combined preheating by SNe and AGNs yields entropy levels corresponding to 100 keV cm^2. This is raised to 180 keV cm^2 by the internal blast driven by a quasar deriving from a BH of $10^9 \, M_\odot$ with coupling $f \approx 5 \times 10^{-2}$ that produces $\Delta E/E \approx 1$. The resulting central entropy $K_{0.1}$ including the appropriate T-dependent shape factor is shown by the solid and dashed lines in Figure 4 for both models, ejection and outflow, discussed above.

Relatedly, the entropy profiles are *steep* after the blast passage. They arise when the entropy produced in the blast, clearly piled up toward the leading shock, is redistributed in the recovered equilibrium. We find
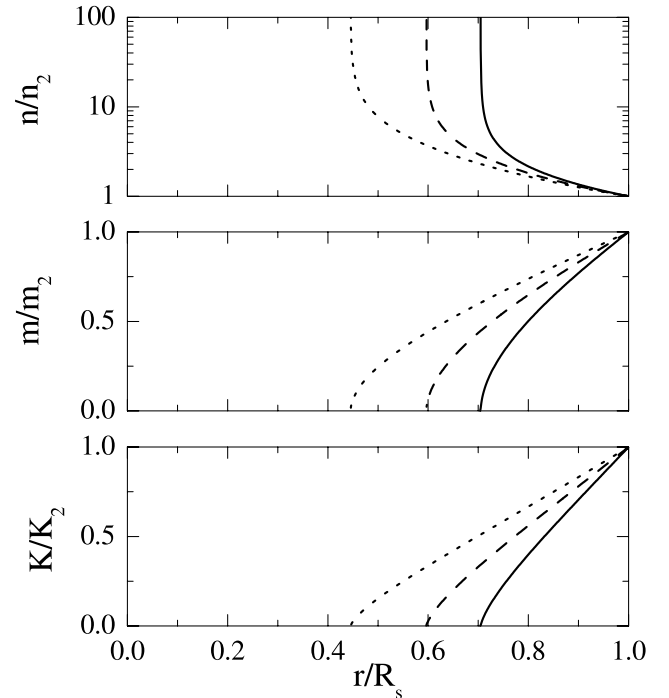
$$\kappa(m) \propto m^{4/3} \qquad (9)$$

FIG. 6.—Distributions of density (*top*), cumulative mass (*middle*), and entropy (*bottom*) within the blast, computed from eqs. (C9) and (C10) for $\omega = 2$ and normalized to their postshock values. Solid lines are for a strong shock with $\Delta E/E = 3$, dashed lines are for an intermediate shock with $\Delta E/E = 1$, and dotted lines are for a weak shock with $\Delta E/E = 0.3$.

to hold in terms of the plasma mass m swept up by the blast (see Fig. 6 and eq. [C11]). In the adiabatically recovered equilibrium we require the entropy distribution $\kappa'(m)$ to equal $\kappa(m) \propto m^{4/3}$ and proceed in analogy with the technical steps used in § 3.

In detail, let us approximate $\kappa' \propto r^\alpha$, with α to be determined; then equation (A3) implies $n' \propto r^{-3(\alpha+2)/5}$, and thus $\kappa' \propto m^{5\alpha/3(3-\alpha)}$ follows. Requiring this to be consistent with the entropy distribution $\kappa \propto m^{4/3}$ in the blast (as anticipated above) yields $\alpha \approx 1.3$. In other words, the blast acting from inside leaves in the readjusted plasma a strong imprint of its own entropy distribution, in the form of a *steep* profile $\kappa'(r) \propto r^{1.3}$ consistent with the data.

6. DISCUSSION AND CONCLUSIONS

In this paper we have used pilot semianalytic modeling to show that the energy fed back to baryons by AGNs and quasars is essential to fit the recent X-ray data. We find that the AGN external preheating dominates over SNe to yield the scaling laws $L_X \propto T^3$ and $K \propto T^{2/3}$ related by equation (1) that constitute fitting trends in clusters if still marginal for groups. But in groups and in large galaxies the quasar impulsive feedback acting from the inside takes over, to eject some plasma and further *depress* L_X, while *enhancing* K and originating *non-isentropic* profiles.

We stress that the energy added by AGNs plays an *inverse* role in preheating and in ejection/outflow. This is because in moving from clusters to groups the ratio $\Delta E/E$ of the added versus the equilibrium energy is bound to increase. This causes relatively higher external preheating, warmer inflows, and *weaker* accretion shocks; on the other hand, it drives *stronger* internal blasts, causing more mass ejection/outflow. In parallel, the leading shocks of the blasts replace the accretion shocks in the role

of increasing the outer entropy production, thus originating comparably steep entropy profiles.

Such internal effects, however, are to *saturate* in galaxies because the values of $\Delta E/E$ there are limited, lest the impulsive quasar feedback ejects so much of the surrounding baryons as to stop the BH accretion altogether (see Silk & Rees 1998); the saturation is what in our calculation yields the lower *elbows* of the solid and dashed lines presented in Figure 3. As argued in Cavaliere et al. (2002), the system constituted by the BH and the surrounding baryons self-regulates to the verge of unbinding; the condition $\Delta E \approx E$ directly yields $M_\bullet \approx 5 \times 10^8 \, M_\odot (f/5 \times 10^{-2})^{-1} (\sigma/300 \, \mathrm{kms}^{-1})^5$ in terms of the DM velocity dispersion σ. In turn, the latter is found to correlate less than linearly with the velocity dispersion σ_* of the host galactic bulge (Ferrarese 2002; Baes et al. 2003; A. Pizzella et al. 2005, in preparation); so the BH mass approaches $M_\bullet \propto \sigma_*^4$.

Thus for the *same* value $f \approx 5 \times 10^{-2}$ indicated by the average X-ray data for groups we agree (within the observed scatter; see Tremaine et al. 2002) with the observations of the uppermost relic BH masses in the bulges of many local and currently inactive galaxies. Similar BH masses may be also contributed by an initial, supercritical accretion phase (as discussed by King 2003), launching the piston that in turn drives the far-reaching blasts described above. Subsequently, our outgoing self-similar blasts with $\Delta E(t)/E(<R_s) \approx$ const stay tuned to the condition $\Delta E \approx E$. Specifically, for $\omega \to 2.5$ not only $E(<R_s) \propto R_s^{5-2\omega} \to$ const holds but also $\Delta E \propto t^{2(5-2\omega)/\omega} \to$ const applies, consistent with fading quasar output; thus, at most, limited increase of BH mass $M_\bullet$ takes place.

The empirical fact (see Wandel 2002; Vestergaard 2004) that a similar $M_\bullet$-σ correlation appears to hold also for the currently active and faraway BHs is consistent with our adoption of comparable values for $M_\bullet$ energizing both modes of nuclear activity: the impulsive quasar feedback effective for plasma ejection from groups and galaxies, and the smoother, long-lived AGN outputs sufficient to preheat the gas falling into poor clusters. We are also consistent with the rough equality of the mass densities in BHs derived from the powerful emissions of the quasars in the optical band (see Marconi et al. 2004) and from the weaker and later AGN activity detected mainly in X-rays (Hasinger 2004; Fabian 2004a).

On the other hand, strong and rare (i.e., increasingly sporadic) quasar impacts can also explain the *scatter* of the X-ray data widening toward smaller systems as poor groups or massive galaxies (Mushotzky 2004). This we trace back to the increasing *variance* in the occurrence of strong quasar events or even in their coupling level f that concur to dynamically modulate the plasma ejection $\Delta m/m \propto f \, M_\bullet$ and nonlinearly affect $L_X \propto (1 - \Delta m/m)^2$ when $\Delta m/m$ approaches 1. As the hierarchical clustering proceeds toward clusters, instead, the evolution of the quasars cuts down most internal effects; this is because the impulsive contributions to ΔE within a structure's dynamical time can hardly keep pace with the increase of the equilibrium energy $E \propto m T_v$ in such late and massive systems with deep potential wells.

We stress that our upper and lower bounds for L_X illustrated in Figure 3 by the SN strip and the quasar line comprise nearly *all* data points, except for a few groups with peculiar features currently under scrutiny (see Mushotzky 2004; Osmond & Ponman 2004). So we submit that several pieces of data fit together when considering both the external preheating from AGNs and the internal impact from quasars, with the same average values of $f \, M_\bullet$. We remark that several authors (e.g., Ruszkowski & Begelman 2002; Fabian 2004b; Zanni et al. 2004) have argued the relevance of AGN feedback in explaining the puzzle posed by the "cool cores" (Molendi & Pizzolato 2001) at the very centers of many clusters. On the other hand, Cavaliere et al. (2002) and Granato et al. (2004) have stressed that powerful quasar impacts in massive spheroids easily quench star formation and produce precociously red giant elliptical galaxies.

To conclude, we stress that energy feedback from AGNs and quasars with an overall coupling around 5×10^{-2} to the ambient baryons yields agreement with independent observations in different frequency bands and over different distance scales. Specifically, this paper is focused on the extended X-ray emissions and plasma entropy of poor clusters and groups; but we have also considered at galactic and subgalactic scales the mainly optical correlation of nuclear BH masses versus host velocity dispersions. At the intermediate scales of early massive galaxies and in the microwave/submillimeter band, we have proposed in Lapi et al. (2003) how to catch quasar impacts in the act from resolved Sunyaev-Zel'dovich signals enhanced by overpressure in running blast waves. Such transient events sweeping plasma outward to lower densities (see Figs. 5 and 6) hardly increase the extended X-ray emissions; they instead specifically correlate with pointlike X-rays from a fully active quasar and/or with strong IR emissions signaling a nascent quasar enshrouded by dust.

APPENDIX A

HYDROSTATIC EQUILIBRIUM

The hot plasma constituting the ICP/IGP pervades the potential wells of clusters and groups, being in overall virial equilibrium with the DM. As the sound crossing time is comparable to, or somewhat shorter than, the structure dynamical time, hydrostatic equilibrium applies; when the thermal pressure $p = nkT/\mu$ is dominant (see Ricker & Sarazin 2001; Inogamov & Sunyaev 2003), this yields

$$\frac{1}{m_p n} \frac{dp}{dr} = -\frac{d\Phi}{dr}, \tag{A1}$$

in terms of plasma number density n and temperature T. The solution of this differential equation requires one *boundary* condition, for example, the value $n(R) = n_2$ at the virial radius $r = R$; it also requires an equation of state, i.e., a specific relation between $n(r)$ and $T(r)$.

As to the DM potential $\Phi(r)$, we adopt the widely used NFW form (Navarro et al. 1997),

$$\Phi(r) \approx -3\sigma^2 g(c) \frac{\ln(1 + r/r_s)}{r/r_s}, \tag{A2}$$

involving the one-dimensional velocity dispersion σ of the DM and the scale $r_s \equiv R/c$. The concentration parameter $c \approx 5(M/10^{15}\, M_\odot)^{-0.13}$ slowly increases (Bullock et al. 2001), and the factor $g(c) = [\ln(1 + c) - c/(1 + c)]^{-1}$ weakly rises from clusters to groups. To wit, the smaller, earlier DM halos are more concentrated in terms of the normalized potential $\phi \equiv \Phi/\sigma^2$, consistent with the tenets of hierarchical structure formation (see Padmanabhan 2003).

It is useful to recast the hydrostatic equilibrium in terms of the all-important adiabat $K = kT/n^{2/3}$ to obtain

$$\frac{5}{3} \frac{d\ln n}{d\ln r} + \frac{d\ln K}{d\ln r} = -\frac{kT_v}{Kn^{2/3}} \frac{d\phi}{d\ln r}; \tag{A3}$$

recall that $kT_v = \mu m_p \sigma^2$ is the virial temperature. The above is a first-order differential equation of the Euler type for $n(r)$; in terms of $K(r)$, it can be formally integrated by standard methods to obtain equation (2).

In the cluster outskirts, equation (A3) directly relates the slopes of $n(r)$ and $K(r)$, so that $n(r) \propto r^{-3(\alpha+2)/5}$ corresponds to $K(r) \propto r^\alpha$. This is easily derived near $r \approx R$, where for the NFW potential $d\phi/d\ln r \approx 3$ holds; meanwhile, the coefficient $T_v/Kn^{2/3} \approx T_v/T_2$ is easily recognized to be β, with values close to $\frac{2}{3}$ for clusters.

APPENDIX B

ACCRETION SHOCKS AND LAYERS

Across any sharp transition such as a shock, the conservation laws of mass, total stress, and energy for a plasma with 3 kinetic degrees of freedom are written (Landau & Lifshitz 1959)

$$n_1 \tilde{v}_1 = n_2 \tilde{v}_2,$$
$$p_1 + m_p n_1 \tilde{v}_1^2 = p_2 + m_p n_2 \tilde{v}_2^2,$$
$$\frac{1}{2} m_p n_1 \tilde{v}_1^3 + \frac{5}{2} p_1 \tilde{v}_1 = \frac{1}{2} m_p n_2 \tilde{v}_2^3 + \frac{5}{2} p_2 \tilde{v}_2. \tag{B1}$$

As is customary, we have indicated with the subscripts 1 and 2 the pre- and postshock variables, respectively; in addition, by $\tilde{v}$ we indicate velocities measured in the shock *rest* frame.

The previous system of equations leads after some algebra to the temperature jump $T_2/T_1 \equiv \theta$ under the *general* form

$$\theta = \frac{5}{16} \mathcal{M}^2 + \frac{7}{8} - \frac{3}{16} \frac{1}{\mathcal{M}^2}, \tag{B2}$$

in terms of the Mach number $\mathcal{M} \equiv (3\mu m_p \tilde{v}_1^2/5kT_1)^{1/2}$; this is equation (6) of the main text. It is seen that shock heating ($\theta > 1$) requires the flow to be supersonic in the shock rest frame, i.e., $\mathcal{M} > 1$ as expected. The corresponding density jump reads

$$\frac{n_2}{n_1} = \frac{4\mathcal{M}^2}{\mathcal{M}^2 + 3}; \tag{B3}$$

or, in terms of θ (see Cavaliere et al. 1999),

$$\frac{n_2}{n_1} = 2\left(1 - \frac{1}{\theta}\right) + \sqrt{4\left(1 - \frac{1}{\theta}\right)^2 + \frac{1}{\theta}}. \tag{B4}$$

This may be used to express the postshock adiabat $K_2 = kT_2/n_2^{2/3}$, which leads to equation (5) of § 4 in the context of accretion flows. The same general equation also applies to the leading shock of an outgoing blast wave, discussed in § 5.

Focusing now on *accretion* flows, we consider what happens if the transition occurs across a layer of finite thickness δ located at $r \approx R$. In such a case, the conservation equations above include additional terms due to volume forces or nonplanar geometry; e.g., in the momentum equation the gravitational term $\int_{R-\delta}^{R} dr\, GM(<r)n(r)/r$ should be considered. However, these corrections are $O(\delta/R)$ relative to the term $p_1 + m_p n_1 \tilde{v}_1^2$ when $\delta/R \ll 1$ applies; in particular, we have checked this to hold for any reasonable DM and gas distributions $M(<r)$ and $n(r)$ inserted in the above integral.

In fact, for the numerous small merging partners with mass ratio $M'/M \lesssim 5\%$ the diffuse baryonic component is stripped away promptly (i.e., within a layer $\delta/R \lesssim 10\%$) from its DM counterpart and raised to the final temperature and entropy levels (see Tormen et al. 2004). These smaller merging partners with cooler T_v' undergo prompter and also stronger transitions; so they not only are better described by equations (B2), (B3), and (B4), but also dominate the averaging procedure over the distribution of progenitor

masses M' that are used in the main text to compute the effective value of $K_2(T)$. For all these reasons, we refer to "shocks" but imply that similar results also hold for thin layers.

It is useful to relate the inflow velocity $\tilde{v}_1$ in the *shock* rest frame to the infall velocity v_1 in the *cluster* rest frame, to obtain

$$\tilde{v}_1 = \frac{2}{3} v_1 \left[1 + \sqrt{1 + \frac{15}{4} \frac{kT_1}{\mu m_p v_1^2}} \right]; \qquad (B5)$$

here we have assumed the kinetic energy to be small downstream. In turn, the infall velocity v_1 is set by the DM gravitational potential Φ_2 at the virial radius through energy conservation, which yields

$$v_1 = \sqrt{-2\chi\Phi_2}; \qquad (B6)$$

the fudge parameter $\chi = 1 - R/R_f$ expresses the ignorance of the exact position of the radius $R_f \gtrsim R$ at which free fall begins (see Voit et al. 2003). The upper bound $\chi \approx 0.7$ obtains if R_f is computed by equating the free-fall speed to the Hubble flow. In fact, based on many numerical simulations since Bertschinger (1985), we adopt the value $\chi \approx 0.37$, close to that obtained if the gas inflow begins at the turnaround radius during the gravitational collapse of a standard "top-hat" perturbation (see Padmanabhan 2003).

We now derive a number of convenient approximations to the temperature and density jumps valid for very strong, moderately strong, and weak shocks, which are used in § 4 of the main text. For very strong shocks with $kT_1/\mu m_p v_1^2 \ll 1$ that occur for supersonic accretion onto rich clusters, equation (B5) reads $\tilde{v}_1 \simeq 4v_1/3$; thus, equations (B2) and (B4) respectively approximate to

$$\theta \simeq \frac{1}{3} \frac{\mu m_p v_1^2}{kT_1}, \qquad \frac{n_2}{n_1} \simeq 4; \qquad (B7)$$

the former expresses the limit where full thermalization of the inflow kinetic energy takes place. We can now use equation (B6) with $\Phi_2 \approx -5.7\sigma^2$ (the NFW potential corresponding to a concentration $c = 5$) to find $v_1 \approx 2.1(kT_v/\mu m_p)^{1/2}$; putting all of this together yields $\beta = kT_v/\theta kT_1 \simeq 3kT_v/\mu m_p v_1^2 \approx 0.7$, a value consistent with the observations of rich clusters.

For moderately strong shocks with $kT_1/\mu m_p v_1^2 \lesssim 1$ that occur for preheated accretion onto poor clusters, equation (B5) gives $\tilde{v}_1 \simeq 4v_1/3 + 5kT_1/4\mu m_p v_1$. Now equations (B2) and (B4) approximate to

$$\theta \simeq \frac{1}{3} \frac{\mu m_p v_1^2}{kT_1} + \frac{3}{2}, \qquad \frac{n_2}{n_1} \simeq 4\left(1 - \frac{15}{16}\frac{1}{\theta}\right); \qquad (B8)$$

relatedly, the parameter $\beta = T_v/\theta T_1$ is lowered from the cluster value around 0.7 to

$$\beta \simeq 0.7\left(1 - \frac{3}{2}\frac{1}{\theta}\right). \qquad (B9)$$

For weak shocks with $kT_1/\mu m_p v_1^2 \gg 1$ that occur for preheated accretion in small groups, one recovers from equations (B2) and (B4) the adiabatic limit

$$\theta \simeq 1 + \sqrt{\frac{4\mu m_p v_1^2}{15kT_1}}, \qquad \frac{n_2}{n_1} \simeq 1 + \frac{3}{2}(\theta - 1). \qquad (B10)$$

APPENDIX C

A NEW FAMILY OF SELF-SIMILAR BLAST WAVES

Hydrodynamic flows are amenable to a self-similar description when their dynamics can be characterized in terms of space and time variables, and of a small set of parameters with independent dimensions. Although self-similar solutions are only particular descriptions of a hydrodynamic flow, they often accurately yield its actual asymptotic behavior and offer a useful guide for understanding its generic features, as discussed by Zel'dovich & Raizer (1967).

Self-similar solutions have been systematically investigated by Sedov (1959) for blast waves originated by time-dependent energy discharges into a gas with power-law density. Such solutions have then been successfully applied to a variety of astrophysical problems, such as the propagation of SN remnants (see Chevalier 1976) and of shocks driven by solar flares (see Parker 1963). Most of these treatments consider a gas with negligible initial pressure so that the resulting blast wave is strongly supersonic; moreover, they do not include gravitational effects, in particular those due to a dominant DM component.

In the main text we are interested in *strong* and *weak* blasts driven by comparable energy discharges into plasmas in virial equilibrium with the DM at temperatures differing by factors 10^2 from galaxies to clusters. To cover the full range, we derive here (see also Lapi 2004) a new family of self-similar solutions that not only include a power-law initial density gradient and time-dependent energy injection, but also incorporate DM gravity and a finite initial pressure. In Figure 5 we preliminarily outline the unperturbed equilibrium and the perturbed flow.

C1. THE AMBIENT MEDIUM

We consider initial configurations constituted by DM profiles

$$\rho(r) = \rho_R \left(\frac{R}{r}\right)^\omega \tag{C1}$$

with power-law index $2 \le \omega < 5/2$; the case $\omega = 2$ corresponds to the standard isothermal sphere. The plasma is assumed to be in equilibrium within the DM potential well with initial density $n(r) \propto \rho(r)$. Such simple power-law runs will be useful for obtaining self-similar blasts, but also constitute fair piecewise approximations of the plasma distributions expressed by equation (2). The plasma temperature and entropy profiles are given by

$$\frac{kT}{\mu m_p} = \frac{2\pi G \rho_R R^\omega}{(\omega - 1)(3 - \omega)} \, r^{2-\omega}, \qquad K = \frac{2\pi G \mu m_p^{5/3} (\rho_R R^\omega)^{1/3}}{(\omega - 1)(3 - \omega)(m/M)^{2/3}} \, r^{2-\omega/3}; \tag{C2}$$

relatedly, the polytropic index $\Gamma = 2(1 - 1/\omega)$ ranges from 1 to 1.2 when ω increases from 2 to 2.5. The total energy of the gas in equilibrium is

$$E_{\text{tot}}(<r) = \frac{1}{2}\left[-\frac{3}{5}\frac{3-\omega}{5-2\omega}(4\omega - 7)\right]m(<r)c_s^2 \propto r^{5-2\omega}; \tag{C3}$$

here $m(<r) = 4\pi m_p \int^r dx\, x^2 n(x) = 4\pi(m/M)\rho_R R^\omega r^{3-\omega}/(3-\omega)$ is the gas mass within r and the sound speed is $c_s = (5kT/3\mu m_p)^{1/2} \propto r^{1-\omega/2}$. The bounds $2 \le \omega < 2.5$ guarantee the total energy of the system to be finite and negative; hereafter and in the main text we indicate its modulus with $E(<r) \equiv -E_{\text{tot}}(<r)$.

C2. THE BLAST

A blast wave sweeps through the plasma as a result of the energy injections $\Delta E(t)$ by a central source. The ensuing unsteady gas flow is described by the system of partial differential equations

$$\partial_t n + \partial_r(nv) + \frac{2nv}{r} = 0,$$

$$\partial_t v + v\partial_r v + \frac{1}{m_p n}\partial_r p + \frac{GM(<r)}{r^2} = 0,$$

$$(\partial_t + v\partial_r)\frac{p}{n^{5/3}} = 0, \tag{C4}$$

supplemented at the leading shock by the Rankine-Hugoniot boundary conditions. The latter may be derived from the general expressions equations (B1) specialized to the case of *internal* shocks, i.e., taking the preshock flow velocity $\tilde{v}_1$ in the shock rest frame equal to $-v_s$, opposite to the shock velocity. This yields

$$v_2 = \frac{3}{4}v_s\frac{\mathcal{M}^2 - 1}{\mathcal{M}^2}, \qquad \frac{p_2}{p_1} = \frac{5\mathcal{M}^2 - 1}{4}, \qquad \frac{n_2}{n_1} = \frac{4\mathcal{M}^2}{\mathcal{M}^2 + 3}, \tag{C5}$$

in terms of the Mach number $\mathcal{M} \equiv v_s/c_s$. Note that the condition for shock formation and propagation $v_s \ge c_s$ can also be written as $p_2 + m_p n_2 v_2^2 \ge p_1$; i.e., the total stress pushing the shock outward has to exceed the upstream pressure.

The flow described by the above equations will be self-similar if it can be expressed in terms of the variables r and t and of only two more parameters with independent dimensions. One must be the gravitational constant G if gravity effects are to be included; as to the other, we take the quantity $\rho_R R^\omega$ entering the initial state given by equation (C1).

Self-similarity then implies for the law of energy injection:

$$\Delta E(t) \propto G^{(5-\omega)/\omega}(\rho_R R^\omega)^{5/\omega}t^{2(5-2\omega)/\omega}. \tag{C6}$$

The resulting time dependencies of the source output turn out to be interesting; the values of the index ω correspond to luminosities going from a *constant* ($\omega = 2$) to a *spike* ($\omega = 5/2$), the upper range being useful to describe the quasar fading out because of its own feedback on the accreting gas. Since $E(<R_s) \propto R_s^{5-2\omega} \propto t^{2(5-2\omega)/\omega} \propto \Delta E$ holds, it is easily seen that $\Delta E/E$ is constant during the blast motion and thus constitutes the key parameter for labeling the solutions. This comes about because the values of $\Delta E/E$ set the Mach number, i.e., the strength of the shock, as we specify below.

Under self-similarity, equations (C4) are solved along the following lines. First, we use the dimensional parameters of the problem to construct the self-similarity (adimensional) variable $\xi \equiv r/R_s(t)$, where

$$R_s(t) = \left[\frac{5\pi G \rho_R R^\omega \omega^2 \mathcal{M}^2}{6(\omega - 1)(3 - \omega)}\right]^{1/\omega} t^{2/\omega} \propto R(\mathcal{M}t)^{2/\omega} \tag{C7}$$
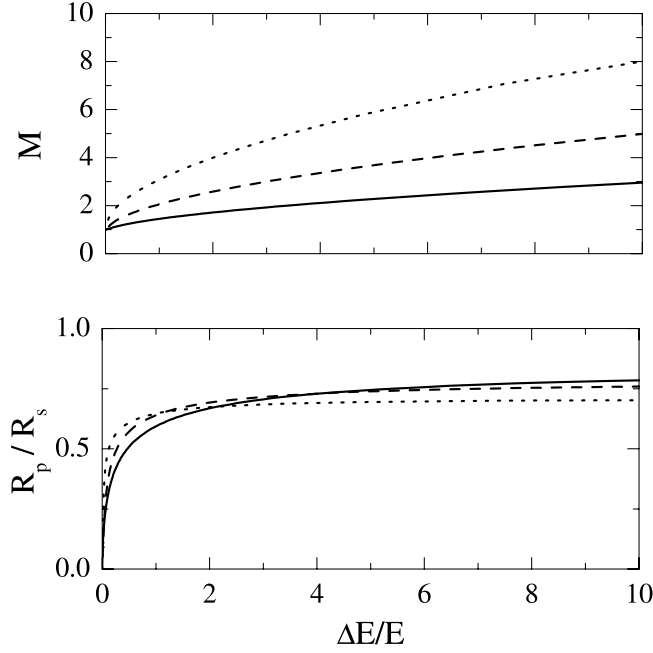
Fɪɢ. 7.—Mach number $\mathcal{M}$ (top) and the piston position $\lambda \equiv R_p/R_s$ (bottom) as a function of $\Delta E/E$. The solid line is for $\omega = 2$, the dashed line is for $\omega = 2.25$, and the dotted line is for $\omega = 2.4$.

is the shock radius. It is now seen that the Mach number $\mathcal{M} = v_s(t)/c_s[R_s(t)]$ is independent of time and position, as is $\Delta E/E$. Note that in our simple model with $\omega = 2$ the blast moves out with constant speed, while for $\omega > 2$ it decelerates.

Then we introduce the adimensional quantities $\mathcal{V}(\xi)$, $\mathcal{D}(\xi)$, and $\mathcal{T}(\xi)$ through

$$v(r, \ t) = \frac{r}{t}\mathcal{V}(\xi), \qquad n(r, \ t) = \frac{1}{m_p G t^2}\mathcal{D}(\xi), \qquad T(r, \ t) = \frac{3\mu m_p}{5k}\frac{r^2}{t^2}\mathcal{T}(\xi); \qquad (C8)$$

these enable us to convert the partial differential equations (C4) into a set of ordinary differential equations:

$$\xi\left[\mathcal{V}' + \left(\mathcal{V} - \frac{2}{\omega}\right)\frac{\mathcal{D}'}{\mathcal{D}}\right] = 2 - 3\mathcal{V},$$

$$\xi\left[\mathcal{V}'\left(\frac{2}{\omega} - \mathcal{V}\right) - \frac{3}{5}\mathcal{T}\left(\frac{\mathcal{T}'}{\mathcal{T}} + \frac{\mathcal{D}'}{\mathcal{D}}\right)\right] = \frac{6}{5}\mathcal{T} + \mathcal{V}^2 - \mathcal{V} + \frac{24}{5}\frac{\omega - 1}{\omega^2\mathcal{M}^2}\xi^{-\omega},$$

$$\xi\left(\mathcal{V} - \frac{2}{\omega}\right)\left(\frac{\mathcal{T}'}{\mathcal{T}} - \frac{2}{3}\frac{\mathcal{D}'}{\mathcal{D}}\right) = -2\left(\mathcal{V} - \frac{1}{3}\right), \qquad (C9)$$

with boundary conditions at $\xi = 1$ ($r = R_s$) given by

$$\mathcal{V}_s = \frac{3}{2}\frac{\mathcal{M}^2 - 1}{\omega\mathcal{M}^2}, \qquad \mathcal{T}_s = \frac{(5\mathcal{M}^2 - 1)(\mathcal{M}^2 + 3)}{4\omega^2\mathcal{M}^4}, \qquad \mathcal{D}_s = \frac{24(m/M)}{5\pi}\frac{(3 - \omega)(\omega - 1)}{\omega^2(\mathcal{M}^2 + 3)}. \qquad (C10)$$

As a last step, we have numerically solved the differential system equations (C9) by using a standard Runge-Kutta integrator with adjustable time step. For various shock strengths we show in Figure 6 the distributions of density, mass, and entropy in the blast for the $\omega = 2$ model.

While the radial mass and entropy distributions differ considerably in the blast and in the initial configuration, the entropy distribution $\kappa(m)$ as a function of the integrated plasma mass $m(<r)$ remains unchanged and reads

$$\kappa(m) \propto m(<r)^{(6-\omega)/3(3-\omega)}. \qquad (C11)$$

The postshock normalization K_2 is raised because of dissipation within the shock, after the *general* equation (5) in the main text that has been derived in Appendix B.

The overall energy balance for the blast flow is written

$$\Delta E(t) - E(< R_s) = 4\pi \int_0^{R_s} dr\, r^2 \left[\frac{1}{2}\, m_p n v^2 + \frac{3}{2}\, p - \frac{GM(<r)}{r}\, m_p n\right]. \tag{C12}$$

This equation relates $\mathcal{M}$ and $\Delta E/E$, and the result is shown in the top panel of Figure 7. Note that for strong shocks $\Delta E/E \propto \mathcal{M}^2$ holds; in particular, such a dependence implies that in the limit $\mathcal{M}^2 \gg 1$ (but in fact already for $\mathcal{M}^2 > 3$) our family of self-similar blast waves converge to the standard solutions with negligible gravity and zero initial gas pressure. For example, for $\omega = 2$ and constant source luminosity one has $R_s \propto \mathcal{M}t \propto (\Delta E/E)^{1/2}t$; since $E \propto R_s$ holds, one recovers the shock motion $R_s \propto L^{1/3}t \propto \Delta E^{1/3}t^{2/3}$, provided by the standard blast wave theory in the strong shock limit. As another example, consider $\omega = 2.5$ and spiky energy liberation after equation (C6), for which one has $R_s \propto \mathcal{M}^{4/5}t^{4/5} \propto (\Delta E/E)^{2/5}t^{4/5}$; since now $E = \mathrm{const}$ holds, one recovers the standard dependence $R_s \propto \Delta E^{2/5}t^{4/5}$ for strong shock.

From Figure 6 it is easily seen that the flow is confined within a shell that terminates at the leading shock at R_s and begins at a trailing "piston," the contact discontinuity located at $R_p = \lambda R_s < R_s$ where the action of the source is transferred to the plasma. Self-similarity implies the thickness $1 - \lambda$ of such a shell to depend only (and inversely) on the shock strength; λ is plotted versus $\Delta E/E$ in the bottom panel of Figure 7.

Analytic approximations may be derived for the limiting behavior of the adimensional variables $\mathcal{V}$, $\mathcal{D}$, and $\mathcal{T}$ in the vicinity of the piston. For a given ω such limiting behaviors turn out to be independent of the shock strength and read

$$\mathcal{V}_p \simeq \frac{2}{\omega} - \frac{6}{5}\left(\frac{7}{\omega} - 2\right)\left(\frac{\xi}{\lambda} - 1\right), \qquad \mathcal{D}_p \propto \left(\frac{\xi}{\lambda} - 1\right)^{(\omega-6)/3(7-2\omega)}, \qquad \mathcal{T}_p \propto \frac{1}{\mathcal{D}_P}. \tag{C13}$$

Thus at the inner piston the density diverges weakly but the mass vanishes (so the overall effects of radiative cooling are negligible), while the temperature goes to zero, making up a finite pressure.

C3. THE SHELL APPROXIMATION

Since the perturbed flow is confined within a shell of constant thickness λ between the inner piston and the leading shock, it is convenient to represent our solutions by using the *shell* approximation (see Cavaliere & Messina 1976; Ostriker & McKee 1988). Here we improve on the classic treatment by extracting the value of the shell thickness λ directly from the exact solution (see Fig. 7) in order to obtain results reliable to better than 15%.

The equation of motion for the shell is written

$$\frac{d}{dt}[m(< R_s)v_2] = 4\pi R_s^2[\langle p\rangle - p_1] - \frac{3-\omega}{5-2\omega}\,\frac{GM(<R_s)}{R_s^2}\,m(<R_s); \tag{C14}$$

here $\langle p\rangle$ is the volume-averaged pressure, which as a function of $\mathcal{M}$ reads

$$\frac{\langle p\rangle}{p_1} = \frac{5}{8}\,\frac{8-3\omega}{3-\omega}\,(\mathcal{M}^2 - 1) + \frac{3}{5-2\omega}. \tag{C15}$$

For weak shock with $\mathcal{M} \to 1$ we obtain $\langle p\rangle/p_1 = 3/(5 - 2\omega)$, while in the strong shock limit $\mathcal{M} \gg 1$ our result $\langle p\rangle/p_1 \to 5\mathcal{M}^2(8 - 3\omega)/8(3 - \omega)$ matches that known for standard, strong blast waves without gravity (e.g., Cavaliere & Messina 1976).

Integrating equation (C14) leads to

$$\Delta E(t) - E(< R_s) = \frac{1}{2}\,m(<R_s)v_2^2 + \frac{3}{2}\,\langle p\rangle V - \frac{3-\omega}{5-2\omega}\,\frac{GM(<R_s)}{R_s}\,m(<R_s), \tag{C16}$$

in terms of the shell volume $V = 4\pi R_s^3(1 - \lambda^3)/3$; this is the simplified, shell version of equation (C12).

A relevant quantity is the ratio between the kinetic and thermal energy of the blast; inserting equation (C15) into equation (C16), one finds

$$\frac{\Delta E_{\mathrm{Kin}}}{\Delta E_{\mathrm{Th}}} = \frac{3}{2(8-3\omega)(1-\lambda^3)}\,\frac{\mathcal{M}^2-1}{\mathcal{M}^2}. \tag{C17}$$

This is easily seen to vanish in the weak shock limit ($\mathcal{M} \to 1$) and to take on values $3/(16 - 6\omega)(1 - \lambda^3)$ for strong shocks with $\mathcal{M} \gg 1$, as in standard blasts with no gravity.

Finally, we remark that equations (C7), (C15), (C16), and (C17) constitute a set of handy relations useful in the main text and suitable to implement in semianalytic models or hydro+N-body codes of galaxy formation.

LAPI, CAVALIERE, & MENCI

REFERENCES

Allen, S. W., & Fabian, A. C. 1994, MNRAS, 269, 409
Baes, M., Buyle, P., Hau, G. K. T., & Dejonghe, H. 2003, MNRAS, 341, L44
Balogh, M. L., Babul, A., & Patton, D. R. 1999, MNRAS, 307, 463
Bennett, C. L., et al. 2003, ApJS, 148, 1
Bertschinger, E. 1985, ApJS, 58, 39
Blanchard, A., Valls-Gabaud, D., & Mamon, G. A. 1992, A&A, 264, 365
Borgani, S., et al. 2002, MNRAS, 336, 409
Bower, R. G. 1997, MNRAS, 288, 355
Bressan, A., Chiosi, C., & Fagotto, F. 1994, ApJS, 94, 63
Bullock, J. S., et al. 2001, MNRAS, 321, 559
Cavaliere, A., & Fusco-Femiano, R. 1976, A&A, 49, 137
Cavaliere, A., & Lapi, A. 2005, in Joint Evolution of Black Holes and Galaxies, ed. M. Colpi, V. Gorini, F. Haardt, & U. Moschella (Bristol: IOP), in press
Cavaliere, A., Lapi, A., & Menci, N. 2002, ApJ, 581, L1
Cavaliere, A., Menci, N., & Tozzi, P. 1999, MNRAS, 308, 599
Cavaliere, A., & Messina, A. 1976, ApJ, 209, 424
Chartas, G., Brandt, W. N., & Gallagher, S. C. 2003, ApJ, 595, 85
Chevalier, R. A. 1976, ApJ, 207, 872
David, L. P. 1997, ApJ, 484, L11
De Grandi, S., & Molendi, S. 2002, ApJ, 567, 163
Dos Santos, S., & Doré, O. 2002, A&A, 383, 450
Ettori, S., & Fabian, A. C. 1999, MNRAS, 305, 834
Fabian, A. C. 2004a, in Coevolution of Black Holes and Galaxies, ed. L. C. Ho (Cambridge: Cambridge Univ. Press), 447
———. 2004b, in AIP Conf. Proc. 703, Plasmas in the Laboratory and in the Universe: New Insights and New Challenges, ed. G. Bertin, D. Farina, & R. Pozzoli (New York: AIP), 337
Ferrarese, L. 2002, ApJ, 578, 90
Forman, W., et al. 2004, ApJ, submitted (astro-ph/0312576)
Franceschini, A., Hasinger, G., Miyaji, T., & Malquori, D. 1999, MNRAS, 310, L5
Granato, G. L., De Zotti, G., Silva, L., Bressan, A., & Danese, L. 2004, ApJ, 600, 580
Hasinger, G. 2004, Nucl. Phys. B Suppl. Ser., 132, 86
Horner, D. J. 2001, Ph.D. thesis, Univ. Maryland
Inogamov, N. A., & Sunyaev, R. A. 2003, Astron. Lett., 29, 791
Kaiser, N. 1986, MNRAS, 222, 323
King, A. R. 2003, ApJ, 596, L27
Lacey, C., & Cole, S. 1993, MNRAS, 262, 627
Landau, L. D., & Lifshitz, E. M. 1959, Fluid Mechanics (Oxford: Pergamon)
Lapi, A. 2004, Ph.D. thesis, Univ. Rome "Tor Vergata"
Lapi, A., Cavaliere, A., & De Zotti, G. 2003, ApJ, 597, L93
Lin, Y.-T., Mohr, J. J., & Stanford, S. A. 2003, ApJ, 591, 749
Marconi, A., Risaliti, G., Gilli, R., Hunt, L. K., Maiolino, R., & Salvati, M. 2004, MNRAS, 351, 169
Matteucci, F. 2003, The Chemical Evolution of the Galaxy (Dordrecht: Kluwer)
Mazzotta, P., Markevitch, M., Vikhlinin, A., & Forman, W. R. 2002, in ASP Conf. Ser. 257, AMiBA 2001: High-Z Clusters, Missing Baryons, and CMB Polarization, ed. L.-W. Chen, C.-P. Ma, K.-W. Ng, & U.-L. Pen (San Francisco: ASP), 173
Menci, N., & Cavaliere, A. 2000, MNRAS, 311, 50
Menci, N., Cavaliere, A., Fontana, A., Giallongo, E., Poli, F., & Vittorini, V. 2004, ApJ, 604, 12

Merritt, D., & Ferrarese, L. 2001, MNRAS, 320, L30
Molendi, S., & Pizzolato, F. 2001, ApJ, 560, 194
Muanwong, O., Thomas, P., Kay, S. T., & Pearce, F. R. 2002, MNRAS, 336, 527
Mushotzky, R. F. 2004, in Clusters of Galaxies: Probes of Cosmological Structure and Galaxy Evolution, ed. J. S. Mulchaey, A. Dressler, & A. Oemler (Cambridge: Cambridge Univ. Press), 124
Nath, B. B., & Roychowdhury, S. 2002, MNRAS, 333, 145
Navarro, J. F., Frenk, C. S., & White, S. D. M. 1997, ApJ, 490, 493
Osmond, J. P. F., & Ponman, T. J. 2004, MNRAS, 350, 1511
Ostriker, J. P., & McKee, C. 1988, Rev. Mod. Phys., 60, 1
O'Sullivan, S., Ponman, T. J., & Collins, R. S. 2003, MNRAS, 340, 1375
Padmanabhan, T. 2003, Theoretical Astrophysics, Vol. 3 (Cambridge: Cambridge Univ. Press)
Parker, E. N. 1963, Interplanetary Dynamical Processes (New York: Interscience)
Peebles, P. J. E. 1993, Principles of Physical Cosmology (Princeton: Princeton Univ. Press)
Pipino, A., Matteucci, F., Borgani, S., & Biviano, A. 2002, NewA, 7, 227
Ponman, T. J., Sanderson, A. J. R., & Finoguenov, A. 2003, MNRAS, 343, 331
Pounds, K. A., King, A. R., Page, K. L., & O'Brien, P. T. 2003, MNRAS, 346, 1025
Pratt, G. W., & Arnaud, M. 2003, A&A, 408, 1
Rasmussen, J., & Ponman, T. J. 2004, MNRAS, 349, 722
Ricker, P. M., & Sarazin, C. L. 2001, ApJ, 561, 621
Ruszkowski, M., & Begelman, M. C. 2002, ApJ, 581, 223
Sanderson, A. J. R., & Ponman, T. J. 2003, MNRAS, 345, 1241
Sarazin, C. L. 1988, X-Ray Emissions from Clusters of Galaxies (Cambridge: Cambridge Univ. Press)
Sedov, L. I. 1959, Similarity and Dimensional Methods in Mechanics (New York: Academic)
Silk, J., & Rees, M. J. 1998, A&A, 331, L1
Tormen, G., Moscardini, L., & Yoshida, N. 2004, MNRAS, 350, 1397
Tornatore, L., Borgani, S., Springel, V., Matteucci, F., Menci, N., & Murante, G. 2003, MNRAS, 342, 1025
Tozzi, P., & Norman, C. 2001, ApJ, 546, 63
Tremaine, S., et al. 2002, ApJ, 574, 740
Umemura, M. 2004, in Coevolution of Black Holes and Galaxies, ed. L. C. Ho (Pasadena: Carnegie Obs.), http://www.ociw.edu/ociw/symposia/series/symposium1/proceedings.html
Valageas, P., & Silk, S. 1999, A&A, 350, 725
Vestergaard, M. 2004, ApJ, 601, 676
Voit, G. M., Balogh, M. L., Bower, R. G., Lacey, C. G., & Bryan, G. L. 2003, ApJ, 593, 272
Voit, G. M., & Bryan, G. L. 2001, Nature, 414, 425
Wandel, A. 2002, ApJ, 565, 762
White, S. D. M., Navarro, J. F., Frenk, C. S., & Evrard, A. E. 1993, Nature, 366, 429
Wu, K. K. S., Fabian, A. C., & Nulsen, P. E. J. 2000, MNRAS, 318, 889
Yamada, M., & Fujita, Y. 2001, ApJ, 553, L145
Zanni, C., Murante, G., Bodo, G., Massaglia, S., Rossi, P., & Ferrari, A. 2004, A&A, submitted (astro-ph/0408555)
Zel'dovich, Ya. B., & Raizer, Yu. P. 1967, Physics of Shock Waves and High-Temperature Hydrodynamic Phenomena (New York: Academic)